Bora Sul
The Henry M. Jackson Foundation for the Advancement of Military Medicine, Inc., Bethesda, MD 20817;
Department of Defense Biotechnology High Performance Computing Software Applications Institute, Telemedicine and Advanced Technology Research Center, United States Army Medical Research and Materiel Command, MCMR-TT, 504 Scott Street, Fort Detrick, MD 21702-5012

Talissa Altes
Department of Radiology, University of Missouri, Columbia, MO 65212

Kai Ruppert
Department of Radiology, University of Pennsylvania, Philadelphia, PA 19104

Kun Qing
Department of Radiology, University of Virginia, Charlottesville, VA 22908

Daniel S. Hariprasad
The Henry M. Jackson Foundation for the Advancement of Military Medicine, Inc., Bethesda, MD 20817;
Department of Defense Biotechnology High Performance Computing Software Applications Institute, Telemedicine and Advanced Technology Research Center, United States Army Medical Research and Materiel Command, MCMR-TT, 504 Scott Street, Fort Detrick, MD 21702-5012

Michael Morris
Graduate Medical Education, Brooke Army Medical Center, Joint Base San Antonio Fort Sam Houston, San Antonio, TX 78234

Jaques Reifman[1]
Department of Defense Biotechnology High Performance Computing Software Applications Institute, Telemedicine and Advanced Technology Research Center, United States Army Medical Research and Materiel Command, MCMR-TT, 504 Scott Street, Fort Detrick, MD 21702-5012
e-mail: jaques.reifman.civ@mail.mil

Dynamics of the Tracheal Airway and Its Influences on Respiratory Airflows: An Exemplar Study

Respiration is a dynamic process accompanied by morphological changes in the airways. Although deformation of large airways is expected to exacerbate pulmonary disease symptoms by obstructing airflow during increased minute ventilation, its quantitative effects on airflow characteristics remain unclear. Here, we used in vivo dynamic imaging and examined the effects of tracheal deformation on airflow characteristics under different conditions based on imaging data from a single healthy volunteer. First, we measured tracheal deformation profiles of a healthy lung using magnetic resonance imaging (MRI) during forced exhalation, which we simulated to characterize the subject-specific airflow patterns. Subsequently, for both inhalation and exhalation, we compared the airflows when the modeled deformation in tracheal cross-sectional area was 0% (rigid), 33% (mild), 50% (moderate), or 75% (severe). We quantified differences in airflow patterns between deformable and rigid airways by computing the correlation coefficients (R) and the root-mean-square of differences (Drms) between their velocity contours. For both inhalation and exhalation, airflow patterns were similar in all branches between the rigid and mild conditions ($R > 0.9$; $Drms < 32\%$). However, airflow characteristics in the moderate and severe conditions differed markedly from those in the rigid and mild conditions in all lung branches, particularly for inhalation (moderate: $R > 0.1$, $Drms < 76\%$; severe: $R > 0.2$, $Drms < 96\%$). Our exemplar study supports the use of a rigid airway assumption to compute flows for mild deformation. For moderate or severe deformation, however, dynamic contraction should be considered, especially during inhalation, to accurately predict airflow and elucidate the underlying pulmonary pathology.
[DOI: 10.1115/1.4043723]

[1]Corresponding author.
Manuscript received January 31, 2019; final manuscript received May 1, 2019; published online July 31, 2019. Assoc. Editor: Ching-Long Lin.

Anders Wallqvist
Department of Defense Biotechnology High Performance Computing Software Applications Institute,
Telemedicine and Advanced Technology Research Center,
United States Army Medical Research and Materiel Command,
MCMR-TT,
504 Scott Street,
Fort Detrick, MD 21702-5012

Introduction

Respiration is a dynamic process accompanied by constant expansion and contraction of the lungs during the breathing cycle. Although changes in lung volume occur mostly in the alveoli and small airways, the large airways, including the trachea and bronchi, undergo deformation during forced exhalation or exercise, when minute ventilation increases. In a healthy lung, deformation of large airways is limited because they maintain their structural integrity with the support of stiff materials, such as cartilaginous rings. However, in cases of excessive dynamic airway collapse or tracheobronchomalacia, large airways may show at least a 50% reduction in tracheal area during labored breathing [1,2]. In such cases, the increasing pleural pressure causes the weakened central airways to narrow, which may exacerbate obstructive symptoms and lead to exercise-induced hyperpnea. Although abnormal dynamic contraction of large airways is most commonly associated with symptoms experienced by chronic obstructive pulmonary disease patients during forced exhalation [3,4], it may be identified in healthy subjects as well [5,6]. For example, some military personnel who complained of exertional dyspnea demonstrated symptomatic excessive dynamic airway collapse during exercise, despite the absence of any apparent underlying pathology in small airways or pulmonary parenchyma [6].

Although previous studies have extensively examined the morphological changes involved in excessive large airway contractions and their associated symptoms [3,4,7,8], the effects of dynamic contraction of the trachea on airflow characteristics have not been studied quantitatively. Computational fluid dynamics (CFD) simulations are useful tools for investigating airflow characteristics and provide detailed insights into the respiratory physiology associated with underlying lung conditions. Previously, a number of studies have used computational models incorporating the structural mechanics of airway walls with and without fluid interactions to investigate the contraction of large airways [9–12]. For example, Xia et al. [10] used a linearly compliant model of a single airway bifurcation between the third and fourth generations to investigate the effects of wall stiffening due to fibrosis on the rate of normal breathing. Malve et al. [11] investigated the mechanism of coughing in a human trachea to improve the efficacy of surgery for patients with endotracheal tubes. Similarly, Hollister et al. [12] used a finite element model of the airway wall to demonstrate that mechanical instability leading to complete airway collapse in tracheobronchomalacia is caused by reduced cartilage and fibrous tissue properties. Each of these models simulated deformation of the bronchial tree by assuming uniform material properties for the airway wall and its surrounding tissues. However, these material properties are not well understood and may vary considerably between locations [13].

Improved high-resolution computed tomography (HRCT) imaging techniques have made it possible to acquire multiple lung images during the breathing cycle. Deformation patterns of the airway, obtained from dynamic lung imaging, have been used to study the development of airflow during breathing cycles [14–18]. These studies circumvented the issues regarding uncertainties in the material properties of the airway walls by prescribing the deformation of the airway in fluid simulations, instead of deriving the structural deformation using fluid–structure-interaction modeling. In addition, by removing the required iterative steps to calculate interactions between solid and fluid elements, this method is computationally more efficient. For example, Ibrahim et al. [17] developed a new algorithm for deforming the airway CFD mesh between two volumetric positions to allow for the simulation of the full breathing cycle, and demonstrated the validity of their deformation algorithm using changes in lung volume as measured by magnetic resonance imaging (MRI). Yin et al. [15] developed a novel algorithm that links local structural variables (regional ventilation and deformation of central airways) to global lung function (total lung volume) over three imaged lung volumes using multidetector row computed tomography (MDCT) images. Using this algorithm, they derived a breathing lung model for CFD simulations. However, these models have only examined gradual changes in the conformation of airways at rest or under deep breathing conditions, because the number of MDCT images that can be obtained from each subject is limited by the radiation dose. Thus, the effects of airway contraction during forced exhalation, which would be expected to have a larger impact on flow obstruction, remain unclear.

In this study, we investigated the effects of dynamic deformation of the trachea on airflow based on imaging data from a single healthy volunteer, and tested the validity of a rigid airway assumption with different degrees of modeled tracheal collapse. Thus, we used hyperpolarized gas MRI and HRCT imaging to experimentally characterize tracheal contraction during forced exhalation. In particular, unlike MDCT imaging, HHe-MRI allowed us to measure multiple lung images at high temporal resolution. Subsequently, we directly modeled dynamic conformational changes of the trachea observed during forced exhalation, and computed the corresponding changes in the airflow characteristics of lung airways. Finally, we compared the effects of airway deformation on airflow for steady inhalation and steady exhalation in which the maximally induced deformation in tracheal cross-sectional area was associated with the following three conditions: *healthy*, *at risk of excessive dynamic airway collapse*, and *excessive dynamic airway collapse*.

Methods

In Vivo Measurement of Breathing Dynamics for a Single Healthy Volunteer. We used HRCT imaging and hyperpolarized gas MRI to obtain dynamic profiles of airway conformation during forced breathing for a single healthy subject. The subject was a 39-yr old female without any active pulmonary symptoms or a history of smoking. Pulmonary function test results were normal;

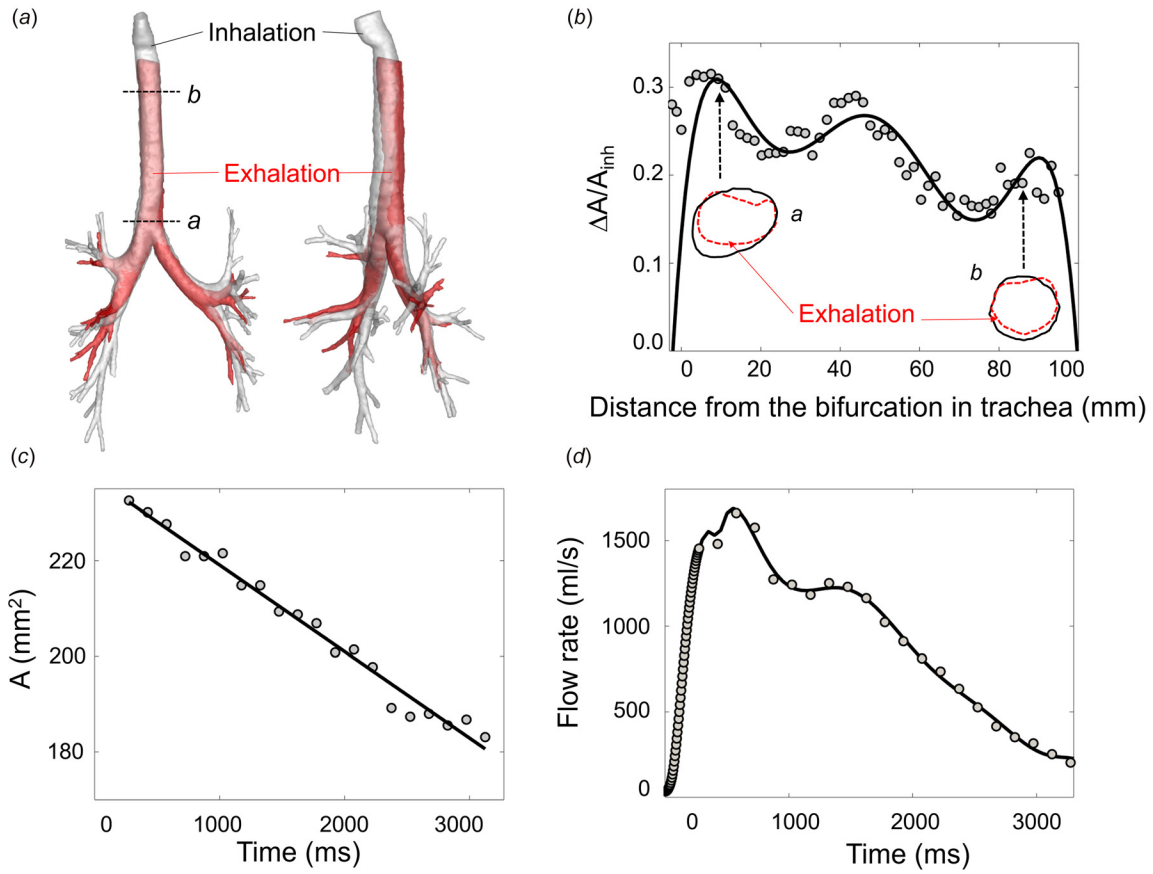

Fig. 1 Dynamic profiles for airway morphology and breathing flow rate during forced exhalation for a healthy subject. Circles show data and solid lines represent fitted curves used as input in computational simulations. (*a*) 3D airway geometry created from HRCT images taken at breath holds after full inflation (light gray) and full deflation (dark gray (print version); red (online version)) of the lung. (*b*) Longitudinal profile of differences in the cross-sectional area of the trachea between inhalation and exhalation (ΔA), normalized by the cross-sectional area of the trachea (A_{inh}) at inhalation, along the trachea using the 3D airway geometry in panel (*a*). The solid line represents the curve fitted to the data (Eq. (1)). The figure also shows outlines of the cross sections of the trachea for inhalation (solid line) and exhalation (broken line) at sections *a* and *b*. (*c*) Time course of the cross-sectional area of the trachea (*A*) during forced exhalation, measured at section *b* using hyperpolarized-He magnetic resonance imaging (HHe-MRI). The solid line represents a linear model fitted to the data (Eq. (2)). (*a*) Flow rate during forced exhalation, measured using a flow meter and HHe-MRI.

the forced expiratory volume measured at one second (FEV_1) was 110% and its ratio to forced vital capacity (FEV_1/FVC) was 90%.

To obtain the airway geometry and the longitudinal profile of changes in tracheal conformation, we collected thin-slice HRCT images of the whole lung at two breath-holding conditions (full inhalation and full exhalation) following a previously described protocol, using a SOMATOM Definition Flash scanner (Siemens, Erlangen, Germany) [19] (Figs. 1(*a*) and 1(*b*)).

To characterize the tracheal conformation as a function of time (Fig. 1(*c*)), we developed a spiral-based, hyperpolarized ^{3}He-MRI technique (HHe-MRI). Following radiofrequency excitation, we applied bipolar flow-sensitization gradients (velocity encoding of 6 m/s) perpendicularly to the imaging slice before the acquisition of each spiral *k*-space interleaf. We inverted the polarity of the flow-encoding gradients after each *k*-space line, which yielded an interleaved flow-encoding pattern. Each spiral acquisition sequence consisted of seven interleaves (two for field-inhomogeneity correction and five for collection of imaging data). Other imaging parameters included the following: the ratio of repetition time to echo time, 10.8 ms/2.9 ms; flip angle, 60 deg; slice thickness, 20 mm; field of view, 50 mm; reconstructed matrix size, 64 × 64. We positioned the axial slice below the larynx but above the lung apices and ran the interleaved acquisition sequence continuously for 50 repetitions. We performed all MR studies at 1.5 T (Avanto, Siemens Medical Solutions, Malvern, PA), using a 32-channel ^{3}He chest radiofrequency coil (RAPID Biomedical, Rimpar, Germany), under a physician's investigational new drug for HHe-MRI. We obtained informed consent, and a physician supervised each study. We polarized Helium-3 gas by collisional spin exchange with an optically pumped rubidium/potassium vapor using a custom-built system, yielding polarizations between 40% and 60%. Image acquisition started at the beginning of inhalation. Subsequently, the subject rapidly inhaled approximately 1 L of HHe through a straw from a Tedlar bag. For forced exhalation, the subject expelled air with effort after first inhaling 1 L of HHe and then holding her breath briefly. Once image acquisition started, the subject exhaled as rapidly as possible. Subsequently, we calculated velocity maps with a temporal resolution of 150 ms from the unwrapped phase difference of each interleaved image pair. We isolated the trachea by thresholding the image intensity maps. We computed the mean flow velocity for a given frame as the average flow value for each pixel weighted by its signal amplitude.

We measured the flow rate of air during forced exhalation (Fig. 1(*d*)), using a flow meter attached to the Tedlar bag. The custom-built flow meter consisted of a mouthpiece, a bag connector, connecting tubes, and a respiratory flow head. Tubes from the flow head were connected to a spirometer (AD instruments, Colorado Springs, CO) for measuring the speed and volume of the flow. The results were further digitalized using an A/D converter (PowerLab, AD instruments, Colorado Springs, CO), and written

to a log file for analysis. Before use, the whole system was calibrated using a standard 3-L spirometer calibration syringe (Hans Rudolph, Inc., Shawnee, KS).

Numerical Calculation of Airflow in Rigid and Contracting Airways

Patient-Specific Boundary Condition. We used patient-specific breathing flow rates (Fig. 1(*d*)) and fractions of air distributed among the lung branches as boundary conditions for CFD simulations. To estimate the fractions of air among the lung branches, we used HRCT lung images taken at two breath-holds—peak inhalation and peak exhalation—as described above. Then, we calculated the air volume distribution among the truncated outlet branches, using the code developed by Dr. Ching-Long Lin and Dr. Eric Hoffman at the University of Iowa, as described in a previous study [19].

Airflows in Rigid and Contracting Airways. We generated three-dimensional (3D) airway geometries for rigid and contracting airways, using data from the healthy subject. For airways at the onset of exhalation, we used HRCT images taken at peak inhalation within the MIMICS software system (version 11, Materialize, Leuven, Belgium) to reconstruct 3D airways from the oral cavity up to the fifth-generation airways. Next, we used our in-house code developed using functions from the Vascular Modeling Toolkit to detect the centerlines of each airway branch and truncate the small airways. Because the length of the trachea differed between inhalation and exhalation by only 3% for the study subject, we performed image registration using the bifurcation point of the trachea as a reference point to compare the cross-sectional area between inhalation and exhalation. Subsequently, we used ICEM CFD (version 14.0, ANSYS, Canonsburg, PA) to generate meshes in the processed airway geometry for CFD calculations. We used hybrid mesh prism layers near the wall and tetrahedral cells at the core, with the cell size changing gradually, being finer near the wall and coarser at the core of the geometry. We performed a grid independence test using coarse meshes (9,412,767 cells) and refined meshes (14,107,876 cells) to ensure that the relative differences in airflow resistance at the trachea between the meshes were less than 0.5%. We used the data obtained with refined meshes to generate the results presented in this study.

To capture the airway deformation during exhalation, we used data on changes in cross-sectional area, which were measured using HRCT and HHe-MRI (circles in Figs. 1(*b*) and 1(*c*), respectively). By fitting mathematical expressions to the data, we obtained the following equations (solid lines in Figs. 1(*b*) and 1(*c*)) for the change in area (ΔA) as a function of the distance x (in meters) from the first bifurcation and the time t (in seconds) after the onset of exhalation

$$\Delta A(x) = a_0 + \sum_{n=1}^{3} (a_n \cos n\omega x + b_n \sin n\omega x) \tag{1}$$

where $a_0 = -2.47 \times 10^6$, $a_1 = 3.66 \times 10^6$, $b_1 = -5.67 \times 10^5$, $a_2 = -1.42 \times 10^6$, $b_2 = 4.50 \times 10^5$, $a_3 = 2.23 \times 10^5$, $b_3 = -1.11 \times 10^5$, and $\omega = -3.12$.

$$\Delta A(t) = -2.27 \times 10^{-1} t - 5.68 \times 10^{-4} \tag{2}$$

Using these equations, we created a user-defined function in FLUENT (version 15.0.7, ANSYS), which prescribes the transient deformation profile of the airway wall along the trachea. At each time-step, we updated the shape of the trachea and meshes by moving the wall boundary set by the user-defined function. For simplicity, we approximated the deformation by isotropically changing the cross-sectional area based on Eq. (2). To solve the flow equations, we used the k–ω SST (Menter's shear stress transport) model and the SIMPLEC method within FLUENT for pressure–velocity coupling, and a second-order scheme for the convective terms. To ensure mesh quality and solution convergence, we used a time-step of 1 μs.

Using 640 processors (2.3 GHz Intel Xeon E5-2698 v3) at the U.S. Department of Defense (DoD) Supercomputing Resource Center, located at the U.S. Army Research Laboratory in Adelphi, MD, we ran the simulations in parallel for 168 h.

Simulation of Steady-State Airflows. We compared steady-state airflows in the rigid airway and airways with tracheal contraction under the following conditions: *healthy*, *at risk of excessive dynamic airway collapse*, and *excessive dynamic airway collapse*. For the healthy condition, the maximal change in cross-sectional area was 33% between peak inhalation and peak exhalation (Fig. 1(*b*)) when the flow rate was 200 ml/s (Figs. 1(*c*) and 1(*d*)). For the at risk of excessive dynamic airway collapse condition, we assumed the tracheal cross-sectional area to decrease to 50%, as reported previously [1,2], while the longitudinal profile of the contraction along the trachea remained the same as that for the healthy condition. For the excessive dynamic airway collapse condition, we assumed the cross-sectional area to decrease by 75%, as previously reported [6,20], uniformly along the trachea. Hereafter, we refer to the conditions, healthy, at risk of excessive dynamic airway collapse, and excessive dynamic airway collapse as mild, moderate, and severe, respectively, as compared to the rigid condition.

To create the airway geometries for the mild and moderate conditions, we simulated airway deformation in FLUENT using prescribed moving boundary conditions without coupling flow equations, until the maximal reductions of cross-sectional area in the trachea reached 33% (mild) and 50% (moderate). For the severe condition, we modified the original geometry in 3-MATIC (version 11, Materialize) by scaling the original cross sections along the trachea.

Quantitative Measure of Airflow Similarity. To assess systematic differences in airflow patterns as a function of the collapsibility of the airway, we quantified the similarity in airflow pattern between each deformable airway and the rigid airway, using Pearson's correlation coefficient (R) and the root-mean-squared differences (Drms) between the velocity values in the cross sections of airway branches normalized by the mean velocity value. To compare the velocity magnitudes A_i and B_i at each point i, we defined R as follows:

$$R = \frac{\sum_i (A_i - \bar{A})(B_i - \bar{B})}{\sqrt{\sum_i (A_i - \bar{A})^2 \sum_i (B_i - \bar{B})^2}} \tag{3}$$

where $\bar{A}$ and $\bar{B}$ denote the mean values over the contours of velocity A and B, respectively. The coefficient R, which measures the linear dependence between two variables, attains values between -1 and 1, with -1 indicating a perfect negative correlation, 0 indicating no correlation, and 1 indicating a perfect positive correlation [21]. If two sets of velocity contours have similar patterns except for their magnitudes, R will be near 1. If the two flow patterns share no similarity, they will be uncorrelated and R will be near zero.

To assess differences in velocity magnitudes between A and B, we calculated Drms, by computing the velocity differences at N grid points of the cross sections and normalizing the differences by the mean velocity of A as follows:

$$\text{Drms} = \frac{\sqrt{\sum_i (A_i - B_i)^2}}{N\bar{A}} \tag{4}$$

The Drms values represent differences in the velocity values between the two lung conditions, relative to the mean velocity of

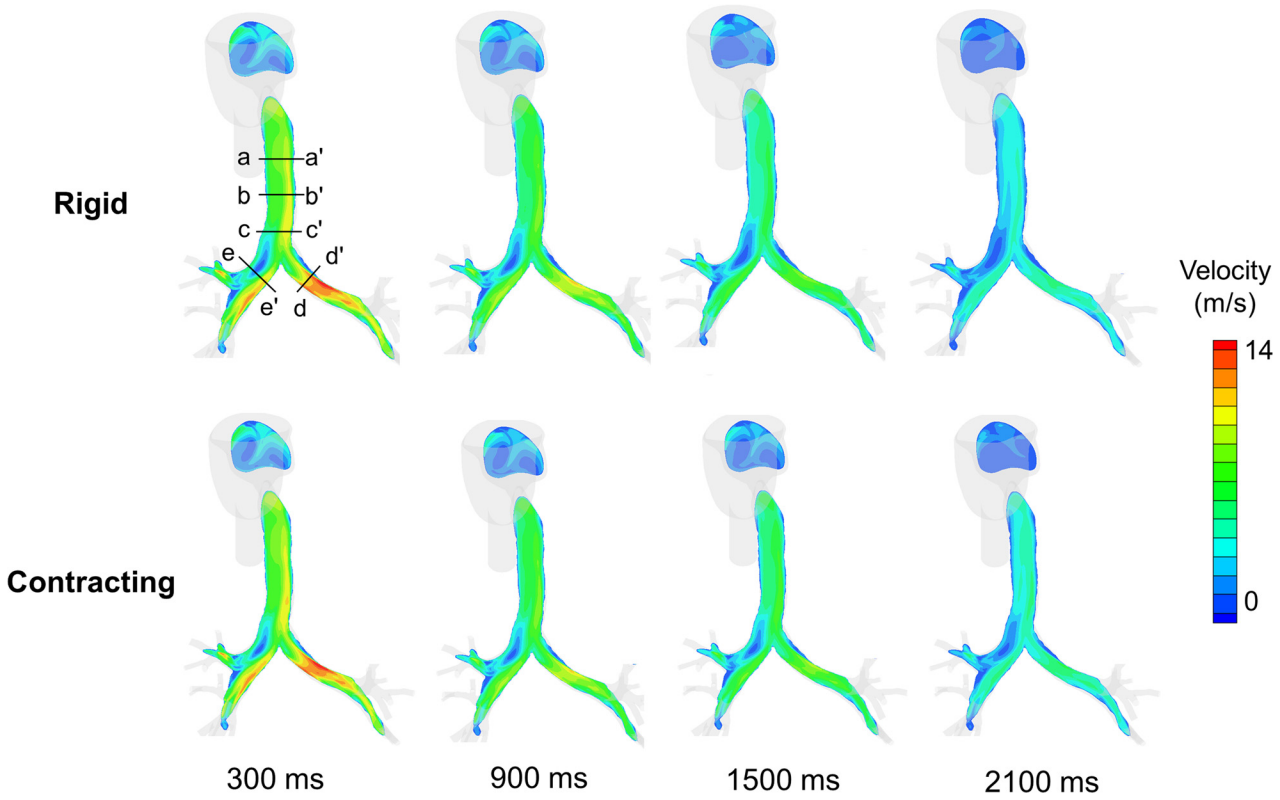

Fig. 2 Comparison of airflow velocity during forced exhalation between a rigid airway and a contracting airway. The rigid airway geometry was obtained from a 3D reconstruction of HRCT images taken at full inflation of the lung. Tracheal deformation in the contracting airway was simulated by imposing longitudinal (Fig. 1(*b*)) and temporal profiles (Fig. 1(*c*)) in user-defined functions in FLUENT (version 15.0.7, ANSYS). In both airways, airflow was simulated using subject-specific flow rates (Fig. 1(*d*)) and flow distribution obtained from HRCT imaging at inhalation and exhalation (as described in the Methods section).

the reference condition. Here, we used MATLAB (R2017a, MathWorks, Natick, MA) to calculate both R and Drms.

To estimate the physiological impact of airway deformation, we calculated the airway resistance and the wall shear stress. The airway resistance is defined as the pressure drop across the inlet and outlet of the airways, divided by the flow rate. The wall shear stress is given by $\mu\partial v/\partial n$, where μ denotes the dynamic viscosity of air and $\partial v/\partial n$ denotes the velocity gradient in the normal direction [22].

Results

Tracheal Contraction. Figure 1 shows the contraction along the trachea and its time course measured during forced exhalation for the study subject. The tracheal cross-sectional area decreased from the point of maximum inflation of the lung to the end of expiration (Fig. 1(*a*)). The change in cross-sectional area decreased nonmonotonically as the distance from the first bifurcation increased (Fig. 1(*b*)). Tracheal contraction peaked near (i.e., 7 mm from) the first bifurcation, showing a 33% change in cross-sectional area. Interestingly, tracheal contraction displayed additional local maxima at the middle and upper sections of the trachea (i.e., 47 mm and 90 mm, respectively, from the first bifurcation). However, there was no bending of the trachea along its length.

Figures 1(*c*) and 1(*d*) show the tracheal cross-sectional area and volume flow rate of breathed air as a function of time at the upper section of the trachea (i.e., 90 mm from the first bifurcation; *b* in Fig. 1(*a*)), during forced exhalation using HHe-MRI. The temporal dependence of the tracheal cross-sectional area, unlike the volume flow rate, was almost linear during forced exhalation, as shown in Eq. (2). The change in cross-sectional area between end-inhalation and exhalation, as measured using HHe-MRI, was 23% (Fig. 1(*c*))—a level consistent with the measurement obtained by comparing HRCT images (Fig. 1(*b*)).

Airflow Pattern During Forced Exhalation in Rigid and Contracting Airways. Using the tracheal contraction and volume flow rate profiles measured from a healthy subject (Fig. 1), we computed and compared airflow patterns during forced exhalation for a contracting airway and a noncontracting (i.e., rigid) airway to examine the extent to which a rigid airway assumption could accurately predict airflow patterns. Figure 2 shows that the velocity patterns were similar between the *rigid* and contracting airways during forced exhalation. At 300 ms after the onset of exhalation, a high-velocity stream developed with flow skewed toward the inner wall of the right bronchus, while flow recirculated at the outer wall near the entrance to the trachea, for both the rigid and contracting airways. In contrast, the velocity profile across the left bronchus was flatter and slightly skewed toward the outer wall for both the rigid and contracting airways. At the junction of the trachea, the high-velocity stream in the left bronchus continued to the left wall of the trachea, while the flow from the right bronchus merged with the momentum directing the left side owing to the curvature of the branch. Consequently, the flow along the trachea was highly skewed at its entrance, while it continued to be skewed toward the left wall.

To identify systematic differences in airflow patterns depending on the degree of airway collapse, we quantified the similarity of the velocity profiles between the rigid and contracting airways by the correlation coefficient R and Drms values. These quantitative analyses showed that differences in airflow patterns between the

Table 1 Correlation coefficients (*R*) and root-mean-square of velocity differences (Drms) for the healthy contracting airway (mild condition) computed against the rigid airway during forced exhalation. Sections a–a′, b–b′, c–c′, d–d′, and e–e′ correspond to those denoted in Fig. 2.

	R				Drms (%)			
Time (ms)	300	900	1500	2100	300	900	1500	2100
a–a′	1.0	1.0	1.0	1.0	3	10	10	13
b–b′	1.0	1.0	1.0	1.0	3	12	12	18
c–c′	1.0	1.0	1.0	1.0	3	14	16	26
d–d′	1.0	1.0	1.0	1.0	3	7	3	3
e–e′	1.0	1.0	1.0	1.0	3	8	3	6

rigid and contracting airways increase during forced exhalation for the trachea, but not for the bronchi.

Table 1 shows that the correlation coefficients were all 1.0 for the velocities at the upper, middle, and lower sections of the trachea (i.e., a–a′, b–b′, c–c′, respectively, in Fig. 2), as well as the sections in the left and right bronchi (i.e., d–d′ and e–e′, respectively, in Fig. 2). Likewise, Drms values at 300 ms were 3% at all sections in the trachea and in the left and right bronchi (Table 1).

The flow skewness was largely due to the geometrical characteristics of the airway branches. The branches immediately upstream of the right bronchus, such as the right upper and right middle branches, had curvatures with similar bending directions. As a result, the flows from these branches merged at the right bronchus with increased momentum toward its inner wall [23]. In contrast, this effect was weaker in the left branch, which was longer and broader. As a result, the flow developed more gradually.

During the course of exhalation, the magnitude of airflow velocity decreased throughout the airways because of the reduction in breathing flow rate (Fig. 1(*d*)). However, the shapes of the velocity contours did not change noticeably. Throughout exhalation, the flow was asymmetric in the right bronchus, traveling with high velocity along its inner wall and recirculating on the other side at the junctions of the right upper branch and trachea. Similarly, the high-velocity domain in the midsection of the left bronchus was present across all time points. For example, a comparison of the velocity values at cross section a–a′ of the contracting airway between 300 ms and 2100 ms revealed a correlation coefficient of 1.0 and a Drms value of 39%.

Moreover, velocity differences between the rigid and contracting airways increased over time, with the largest increases occurring in the trachea. The Drms value increased from 3% at 300 ms to 26% at 2100 ms in tracheal section c–c′, and from 3% at 300 ms to 6% at 2100 ms in section e–e′ of the right bronchus (Table 1). Interestingly, the correlation coefficient remained at 1.0 throughout exhalation at all locations, indicating that the shapes of the velocity contours did not change between the rigid and contracting airways at any location (Table 1).

Comparison Between Zero, Mild, Moderate, and Severe Deformation. To investigate the dynamic airflow characteristics of contracting airways under abnormal conditions, we further extended our analysis to lung conditions that meet, or are at risk of meeting, the criteria for excessive dynamic airway collapse. To compare the airflow characteristics across lung conditions, we examined steady-state airflows with a flow rate of 200 ml/s, which corresponds to that near the end of exhalation and the beginning of inhalation with maximum airway narrowing. At this flow rate, the maximum reduction in tracheal cross-sectional area for the healthy condition was 33% (Fig. 1), which we referred to as mild. For the moderate and severe conditions, we used airway geometries with maximum reductions in the tracheal cross-sectional area of 50% and 75%, respectively. To simplify the computations, we used steady-state flow conditions instead of capturing intermediate states during dynamic conformational changes. We verified that the results from steady-state and transient-state flow conditions were the same (See Supplemental Material on the ASME Digital Collection). This suggested that the system was in a quasi-steady state because the Womersley number was smaller than 1 [24].

Exhalation. Figure 3 shows the steady-state flow patterns of the rigid airway and contracting airways (mild, moderate, and severe). The airways in the rigid and mild conditions showed common flow characteristics, as observed under conditions with dynamic flow rates (Fig. 2), but with increased differences in their velocity magnitudes. Although the tracheal cross-sectional area contracted by up to 33% from that at the onset of exhalation, the correlation between the velocity profiles of the two airways remained at 1.0 for all locations (Table 2). However, compared to conditions with dynamic flow rates, the Drms values increased in the trachea by up to 28%.

The differences between the airflow patterns for the moderate and severe conditions and those for the rigid condition were far greater than the difference between the rigid and mild conditions. Compared to the mild condition, the Drms values computed to compare airflow velocities for the rigid airway with those for the moderate and severe conditions were as much as 70% and 250% higher, respectively (Table 2). However, the flow characteristics determining the shapes of the velocity contours were less sensitive to airway contraction. At the entrance to the trachea, the flow was skewed toward the left side in the presence of multiple local peaks along section c–c′ (Fig. 3, bottom panel). Further downstream, the flow became more symmetric around the center of the trachea along sections a–a′ and b–b′. Owing to these common flow characteristics, the correlation coefficients for the moderate and severe conditions in the trachea were at least 0.9 and 0.8, respectively (Table 2).

Interestingly, for exhalation, the flows in the left and right bronchi were largely insensitive to tracheal contraction for all conditions (Fig. 3, bottom, two rightmost panels). In all conditions, flow was skewed toward the inner wall of the right bronchus, accompanied by flow recirculation at the outer wall near the entrance to the trachea due to the rapidly turning flow from the right upper branch with high curvature (Fig. 3, bottom, rightmost panel). Similarly, the flow in the left bronchus was skewed toward the inner wall, accompanied by flow recirculation at the outer wall, but less noticeably than in the right bronchus (Fig. 3, bottom, second panel from the right). The Drms values at d–d′ and e–e′ were less than 4% and 8%, respectively, and the correlation coefficients were 1.0 for all conditions (Table 2).

Inhalation. Compared to the airflow patterns for exhalation, those for inhalation were more sensitive to airway contraction, especially for the moderate and severe conditions. For both rigid and contracting airways, a jet-like stream of flow formed at the larynx and entered the trachea. However, the travel distance and peak velocity of the stream depended on tracheal contraction. At the upper (a–a′) and middle (b–b′) sections of the trachea, the flow was skewed toward the left side for the rigid and mild conditions. However, this flow asymmetry was less pronounced for the moderate and severe conditions (Fig. 4, top). For the rigid and mild conditions, the difference in the flow pattern increased further downstream in the lower trachea (c–c′), where the jet-like stream split to flow into the left and right bronchi. In contrast, for the moderate and severe conditions, the flow continued to maintain its shape as a single stream, even at the bottom of the trachea. The jet-like stream traveled further for the moderate and severe conditions, likely because the tracheal contraction prevented the stream from being dispersed, and thereby maintained its momentum in the axial direction.

These alterations in the tracheal flow characteristics for the moderate and severe conditions relative to those for the rigid condition are reflected in the correlation coefficients. For the mild

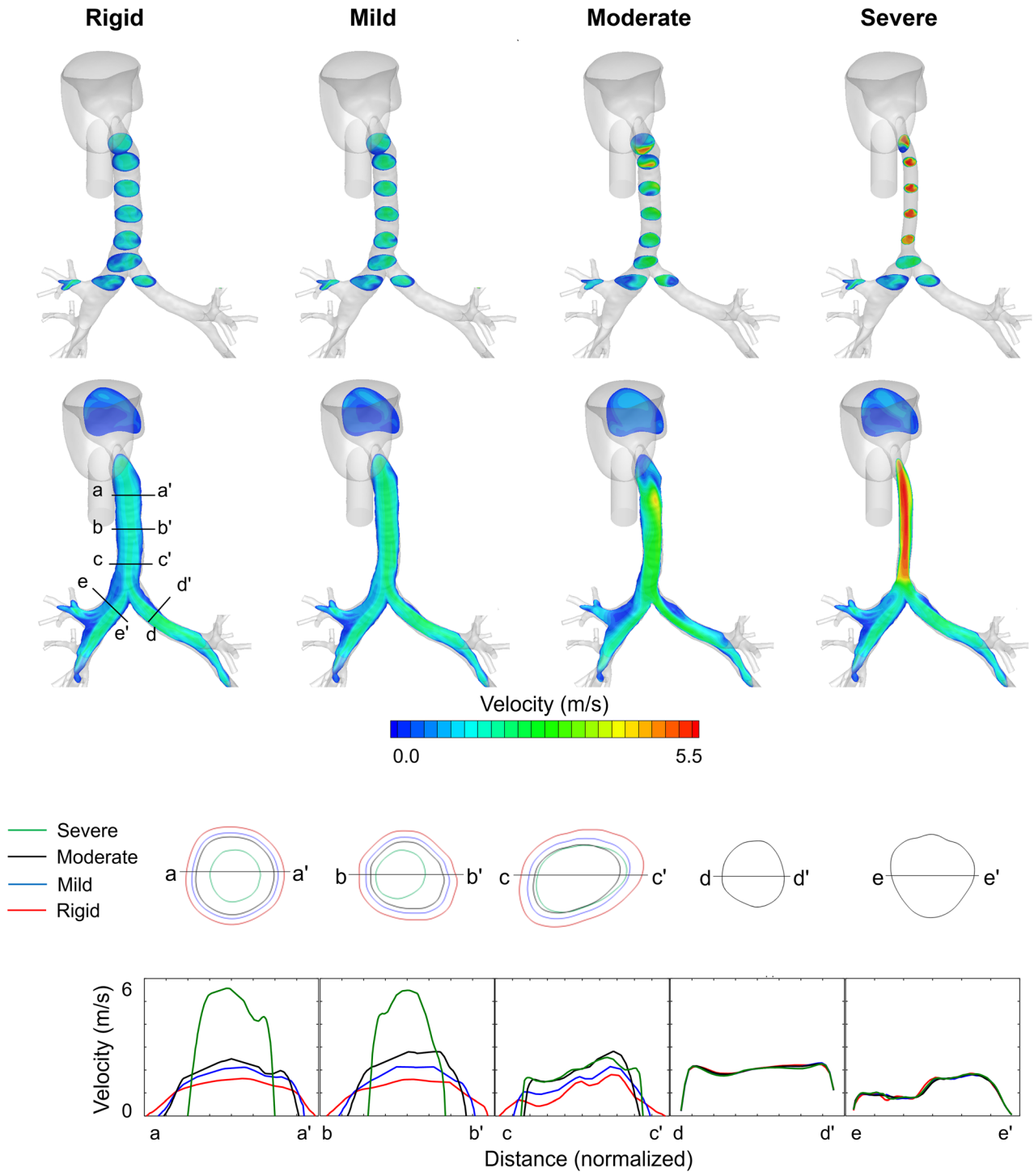

Fig. 3 Comparison of airflow velocity, for steady exhalation at a flow rate of 200 ml/s, between airways showing deformations of 0% (rigid), 33% (mild), 50% (moderate), and 75% (severe) of the maximal change in tracheal cross-sectional area. The panels in the first and second rows show two-dimensional velocity contours in the axial and coronal planes, respectively. The panels in the third row show the cross sections of the airway geometries at a–a′, b–b′, c–c′, d–d′, and e–e′. The panels in the fourth row show velocity magnitudes along sections a–a′, b–b′, c–c′, d–d′, and e–e′.

condition, the correlation coefficients at all sections in the trachea were 1.0, as in the case of exhalation (Table 2). However, for the moderate and severe conditions, the correlation coefficients decreased to as little as 0.1 in the case of inhalation, whereas they were at least 0.8 in the case of exhalation. Likewise, the Drms values at all sections in the trachea were larger during inhalation than during exhalation, especially for the moderate and severe conditions, whereas the Drms values for inhalation (<32%) were similar to those for exhalation (<28%) in the mild condition, they increased in the moderate (<76%) and severe (<96%) conditions (Table 2).

As in the case of tracheal airflow patterns, inhalation airflow in the left and right bronchi differed between the rigid and contracting airways, especially for the moderate and severe conditions. Unlike the airflow patterns during exhalation, those during inhalation differed between the rigid and mild conditions. Interestingly,

Table 2 Correlation coefficients (*R*) and root-mean-square velocity differences (Drms) for the contracting airways computed against the rigid airway at steady inhalation and steady exhalation. Sections a–a′, b–b′, c–c′, d–d′, and e–e′ correspond to those denoted in Figs. 3 and 4.

		R			Drms (%)		
		Mild	Moderate	Severe	Mild	Moderate	Severe
Exhalation	a–a′	1.0	1.0	0.9	22	37	70
	b–b′	1.0	0.9	0.8	27	43	73
	c–c′	1.0	0.9	1.0	28	47	40
	d–d′	1.0	1.0	1.0	2	2	4
	e–e′	1.0	1.0	1.0	7	8	6
Inhalation	a–a′	1.0	0.5	0.2	26	76	75
	b–b′	1.0	0.1	0.6	28	51	75
	c–c′	1.0	0.9	0.7	32	49	79
	d–d′	0.9	0.7	0.4	13	27	38
	e–e′	0.9	0.8	0.4	29	62	96

the correlation coefficients at sections d–d′ and e–e′ were both 0.9 for the mild condition—slightly less than those for exhalation at these locations (both 1.0; Table 2). The changes were more noticeable for the moderate and severe conditions. The correlation coefficients for the moderate and severe conditions at these locations decreased. For example, in section d–d′, the correlation coefficients for inhalation decreased to 0.7 and 0.4 for the moderate and severe conditions, respectively, whereas they were 1.0 for exhalation (Table 2). Moreover, the Drms values in these branches were much larger than those for exhalation in all conditions.

Airway Resistance and Wall Shear Stress for Contracting Airways. Table 3 shows the airway resistance values computed for the rigid and contracting airways at their steady states. The values during exhalation were higher than those during inhalation for all lung conditions. The difference between inhalation and exhalation resistance increased with the degree of airway contraction—they were 12%, 14%, 15%, and 22% for the rigid, mild, moderate, and severe conditions, respectively.

Airway resistance increased with airway contraction. For exhalation, the resistance values of the mild, moderate, and severe conditions increased by 5%, 13%, and 69%, respectively, relative to the resistance of the rigid condition. For inhalation, the corresponding changes were smaller than those for exhalation: the resistance values increased by 3%, 9%, and 52%, respectively, relative to the rigid condition.

Figure 5 shows the wall shear stress values for the rigid and contracting airways at their steady states. In all conditions, the wall shear stress was highest at the larynx in all geometries. This was likely because the sudden narrowing of the larynx increased the velocity gradient of the flow around it. The wall shear stress in the trachea likely increased with increasing airway contraction for the same reason. Relative to the mean wall shear stress of the rigid trachea, the mean wall shear stresses of the trachea in mild, moderate, and severe conditions increased by 32%, 79%, and 404%, respectively, during exhalation. The corresponding changes during inhalation—20%, 45%, and 194%—were smaller than those during exhalation.

Although the mean wall shear stress in the trachea was less than 0.14 Pa for all airway conditions during both steady inhalation and exhalation, their maximum values, in certain regions, were higher than the physiological limit of 0.3 Pa needed to promote respiratory defense mechanisms by enhancing epithelial barrier function [25,26]. During exhalation, the maximum wall shear stress was 0.6 Pa near the larynx for all airway conditions. For all airway conditions, the values during inhalation were higher than those during exhalation. For the rigid, mild, and moderate conditions, the maximum wall shear stress was 2.1 Pa at the upper section of the trachea during inhalation (Fig. 5). For the severe condition, the wall shear stress in the trachea was maximal at the lower section of the trachea during both inhalation and exhalation. For the severe condition, the maximal wall shear stress was 0.4 Pa at a region 20 mm above the first bifurcation during exhalation, and 0.8 Pa at the first bifurcation during inhalation.

Discussion

Airway Dynamics of the Healthy Subject. The cross-sectional area in the trachea decreased almost linearly over time after the onset of exhalation, regardless of the breathing flow rate. In addition, tracheal contraction continued at the same rate of areal reduction, whereas the flow rate decreased more gradually toward the end of exhalation. These data indicate that tracheal contraction was less sensitive to breathing efforts than the flow rate, presumably because of the delay in the response of the tracheal wall to the transmembrane pressure.

Several computational studies have assumed that changes in conformation occur in small airways [27–29]. These studies modeled the small airways as a network of trees with branch resistance and compliance, which determine the phase shift between the pressure load and the conformational change. For large airways, previous studies have employed fluid–structure interaction or other methods to investigate their dynamics and accompanying flow characteristics, assuming uniform material properties along the airway [9–12]. The change in airway conformation, however, was not uniform along the trachea in our study (Fig. 1(*b*)). For example, the tracheal area showed local maxima at multiple locations, at the lower, middle, and upper sections of the trachea as reported in previous studies [30,31]. This suggests that the mechanical properties of the airway may be heterogeneous, as was observed in an earlier in vitro study [13]. Moreover, it is likely that the airway will be stiffened or weakened in a localized manner, when inflammation or fibrosis occurs depending on the disease. Thus, the assumption of uniform material properties may be inadequate for investigations of local disease-induced abnormalities. In addition, the material properties of the airway wall in vivo may differ from those measured in vitro.

It is possible to overcome uncertainty in airway material properties by adopting imaging techniques and using them directly to compute airflows. For example, previous studies have investigated airway dynamics by taking multiple images during breathing maneuvers with the aid of low-dose HRCT imaging [15,17]. These studies examined conformational changes and accompanying airflow patterns in the central airway for light or deep breathing conditions. Imaging deformation during fast breathing conditions, however, requires high temporal resolution and scanning of multiple images during breathing. This presents a challenge for regular computed tomography (CT) scanners, which can take only a limited number of images per session to keep the overall radiation dose within the allowed limit for a subject. Because we did not have access to a newly developed CT scanner that allows imaging of airway deformation at high spatiotemporal resolution with very low radiation (i.e., 0.15 mGy) [5], we used HHe-MRI to measure conformational changes at a high temporal resolution (150 ms) and thereby monitor airway dynamics during forced breathing maneuvers, on the assumption that airway deformation can be accurately measured by both MRI and CT. Compared to other dynamic breathing studies that used CT alone to capture deformation patterns [9,16,17], our method made it possible to take images at multiple time points without exposing the subject to radiation. In addition, the dynamic patterns of airway conformation allowed us to infer the material properties of the airway wall in vivo through fluid–structure-interaction simulations.

Sensitivity of Airflow to Airway Contraction. In this study, tracheal contraction during forced exhalation had minimal influence on the airflow patterns for the healthy condition. Interestingly, even when contraction was maximal near the end of

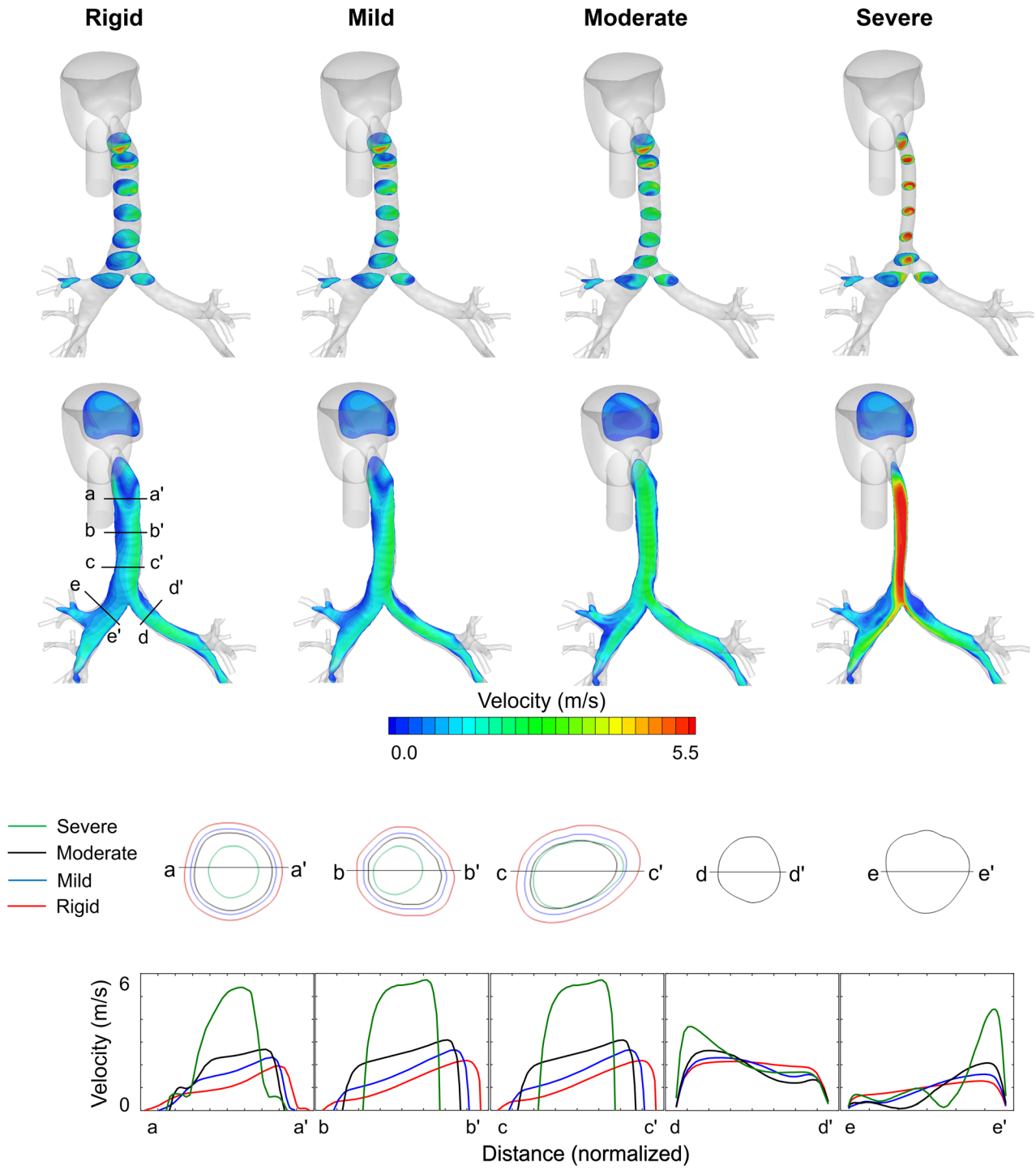

Fig. 4 Comparison of airflow velocity, for steady inhalation at a flow rate of 200 ml/s, between airways showing deformations of 0% (rigid), 33% (mild), 50% (moderate), and 75% (severe) of the maximal change in tracheal cross-sectional area. The panels in the first and second rows show two-dimensional velocity contours in the axial and coronal planes, respectively. The panels in the third row show the cross sections of the airway geometries at a–a′, b–b′, c–c′, d–d′, and e–e′. The panels in the fourth row show velocity magnitudes along sections a–a′, b–b′, c–c′, d–d′, and e–e′.

exhalation and beginning of inhalation, flow characteristics, such as the size of flow recirculation or flow asymmetry, were nearly the same between the rigid and contracting airways for the healthy condition. This suggests that, to study airflow characteristics, the airway dynamics can be simplified by assuming that the trachea remains rigid during forced breathing, even under the mildly deforming conditions.

During exhalation, the changes in flow patterns were localized within the trachea and to a lesser extent in the main bronchi. For example, the velocity magnitudes in the left and right bronchi changed only slightly: the Drms values were less than 8% in both left and right bronchi for any condition, and the shapes of the velocity contours did not differ for any airway (i.e., the correlation coefficient was 1.0), even at sections near the trachea. This suggests that as far as velocity profiles are concerned, the effects of tracheal contraction can be ignored in all lung airways except the trachea.

However, during inhalation, tracheal contraction had large effects on airflow patterns in the trachea as well as in the lower generation airways. The changes in airflow during inhalation were

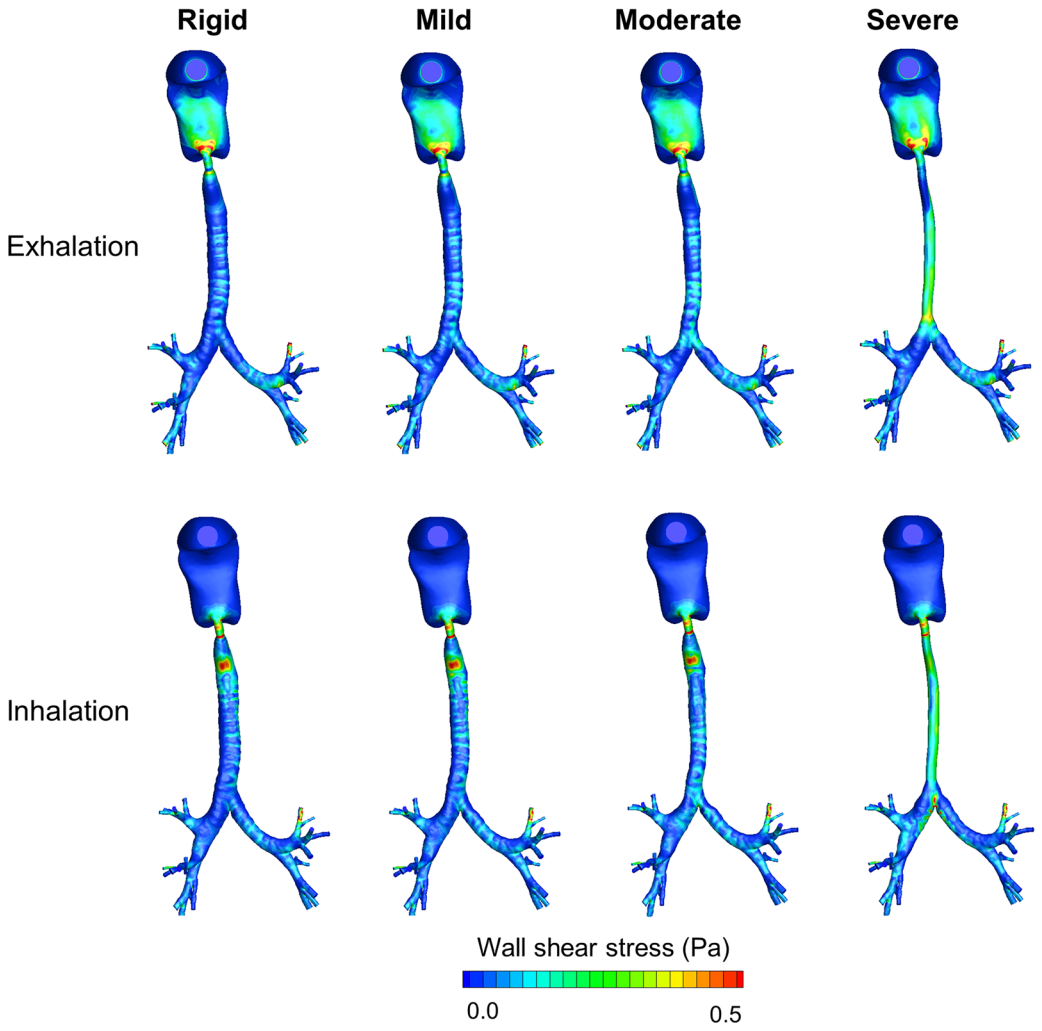

Fig. 5 Comparison of wall shear stress, for steady exhalation and inhalation at a flow rate of 200 ml/s, between airways showing deformations of 0% (rigid), 33% (mild), 50% (moderate), and 75% (severe) of the maximal change in tracheal cross-sectional area

Table 3 Airway resistance (Pa·s/l) during steady inhalation and steady exhalation

	Rigid	Mild	Moderate	Severe
Exhalation	93	98	105	156
Inhalation	83	86	91	128

also more noticeable for contractions in the moderate and severe conditions, where the correlation coefficients fell to as low as 0.1 and 0.2 in the trachea and 0.7 and 0.4 in the left bronchus. In addition, the Drms values in the right bronchus were as high as 62% and 96% for the moderate and severe conditions, respectively. Large deviations of airflow patterns in the moderate and severe conditions suggest that, if tracheal contraction during inhalation leads to a change in cross-sectional area of greater than 50%, then tracheal dynamics should be taken into account when investigating flow. In particular, the large deviation of airflow patterns for moderate to severe contractions suggests that, in contrast to most computational models that assume rigid airways to predict drug delivery patterns [32–34], airway contraction should be considered in the design of drug inhalers. More generally, our findings suggest that as disease severity increases, the effect of airway contraction on airflow patterns during inhalation will increase and, hence, the efficacy of disease interventions using inhaled drugs will become increasingly dependent on airway contraction.

In addition to improving inhaler designs, the results of this study can be used to improve medical interventions for tracheomalacia or excessive dynamic airway collapse, each of which involves narrowing of the airways during expiration. Although dynamic imaging has proven to be effective in the diagnosis of these diseases, understanding airflow function and behavior would be of interest to researchers and clinicians for assessment and diagnosis. Using an image-based CFD study, one can assess the mechanical properties of the airway wall in vivo, which are otherwise unmeasurable. This is particularly important for patients with collapsible airways because the mechanical properties of such airways are expected to differ from those of normal airways and be directly associated with pathological behavior. Estimates of the material properties can be used to improve our understanding and to develop medical interventions for tracheomalacia and excessive dynamic airway collapse.

Limitations of the Study. Our study has a number of potential limitations. First, we investigated the effects of tracheal contraction on airflow characteristics without considering other morphological changes that could affect airflow patterns. For example, we did not consider the effects of off-plane bifurcation angles at the first bifurcation, which were 15 deg and 20 deg at peak exhalation and inhalation, respectively. Nevertheless, a previous study

showed that a 5-deg difference between the two breathing conditions did not result in any noticeable differences in flow patterns [35]. As another example, we did not consider global morphological changes in airway conformation, which are expected to occur in severe diseases. Because the focus of this study was to investigate the effects of tracheal contraction during forced exhalation, we experimentally measured and computationally simulated physiological patterns of tracheal contraction, and did not consider the narrowing of smaller airways. However, the contraction of smaller airways is non-negligible, especially in patients with severe asthma—a condition that involves spontaneous soft-muscle contraction and narrowing of small airways during an asthma exacerbation [4]. Under such circumstances, the airflow characteristics in the smaller airways will deviate even further from those in the case where the airways are assumed to be rigid. It will be difficult to image the exact conformational changes of individual branches under such conditions using current imaging techniques. Nonetheless, newer techniques, such as HHe-MRI and HRCT imaging, may make it possible to monitor global changes in flow conduction [36–38].

Second, we used the same boundary conditions derived from the healthy condition to investigate airflow under the rigid and all contracting airway conditions. However, the distribution of flow among the lung lobes differs between healthy and chronic obstructive pulmonary disease conditions, and airflow patterns are sensitive to those boundary conditions [23]. Thus, the airflow patterns for diseased conditions differ even further from those for the healthy condition, as predicted in this study.

Third, we approximated the airway deformation by isotropically contracting the trachea in the axial plane. However, contraction often occurs through invagination of the posterior membrane of the trachea [39,40]. We tested the validity of our approximation by comparing airflow patterns between isotropic deformation and asymmetric invagination of the posterior membrane. Within the mild deformation range, the change in flow patterns was negligible, justifying the approximation (data not shown). However, the effects of asymmetric contraction increased as the extent of the deformation increased (data not shown). This highlights the importance of detailed investigations on airway deformation under moderate to severe deformation conditions.

Fourth, the accuracy of the cross-sectional area measurement was limited by the spatial resolution and signal intensity of the HHe-MRI. In this study, we achieved a spatial resolution of $0.8 \times 0.8\,\text{mm}^2$, whereas the airway area ranged between $180\,\text{mm}^2$ and $240\,\text{mm}^2$ during the entire breathing period. This allowed us to observe the deformation of the cross section with sufficient temporal and spatial resolution. However, the measurement uncertainty increased toward the end of the breathing period as the signal intensity of HHe-MRI decreased. In a follow-up study, we found that we could improve the signal-to-noise ratio by optimizing the flow sensitivity of the MR pulse sequence against the maximum flow rate (data not shown). This suggests that we can further enhance measurement accuracy by customizing areal measurement depending on the subject's breathing flow rate, which can be determined by spirometric pulmonary function tests.

Finally, our investigation was an exemplar study of airflows based on data obtained from one subject. However, airway geometry shows substantial interindividual variability. For example, tracheal size depends on demographic variables, such as the height and sex of the subject [41]. This variability in airway geometry will affect airflow and particle transport patterns for individual subject [9]. Nevertheless, the deformation profile we used in this study to investigate airflow sensitivity was similar to the representative deformation patterns observed in other disease cases. In particular, it has been observed in both this study and studies of other diseases that, airway narrowing increases at lower levels of the trachea, with local maxima at the middle and lower sections [30,31]. Thus, the sensitivity of airflow patterns to tracheal deformation we observed here may also apply to other healthy and disease cases, unless peculiarities in certain cases markedly alter airway deformation patterns. In fact, consistent with our observations, previous studies have shown that deviation in flow patterns is small under mild breathing conditions with a low flow rate and mild airway deformation [9,17]. Under different patterns of airway deformation, a more accurate assessment of airway deformation may be necessary to evaluate the effectiveness of treatments, such as tracheal stent placement.

Conclusions

In this study, we performed dynamic in vivo lung imaging to characterize patterns of airway deformation during forced exhalation for one healthy subject. We then used the observed deformation patterns to model subject-specific tracheal contractions and assessed their effects on airflow characteristics during forced exhalation. Finally, we compared the flow patterns between airways undergoing varying degrees of deformation, corresponding to different lung conditions for inhalation and exhalation. Using this exemplar case, we showed that the airflow patterns for a healthy condition with mild tracheal deformation approximated those for the rigid airway during both inhalation and exhalation. However, airflow patterns for diseased conditions markedly differed from those for the rigid airway condition, particularly during inhalation. Our findings suggest that if we consider other disease-specific features, such as uneven flow distribution among the lung lobes and possibly increased contraction in other lung branches, the flow patterns and patterns of material transport in diseased conditions will further deviate from those in the healthy condition. This observation highlights the need for using disease-specific models to investigate airflow characteristics and drug delivery designs.

Acknowledgment

High-performance computing resources were made available by the U.S. DoD High Performance Computing Modernization Program. The authors thank Dr. Ching-Long Lin and Dr. Eric Hoffman for providing the HRCT imaging protocol and analysis software for subject-specific flow distribution.

The opinions and assertions contained herein are the private views of the authors and are not to be construed as official or as reflecting the views of the U.S. Army, the U.S. DoD, or The Henry M. Jackson Foundation for Advancement of Military Medicine, Inc. This paper has been approved for public release with unlimited distribution.

Funding Data

- U.S. DoD Health Program, managed by the Military Operational Medicine Program Area Directorate (Funder ID: 10.13039/100000090).
- U.S. Army Medical Research and Materiel Command, Fort Detrick, MD (Funder ID: 10.13039/100000182).
- U.S. Army's Network Science Initiative (Funder ID: 10.13039/100006754).

References

[1] Buitrago, D. H., Wilson, J. L., Parikh, M., Majid, A., and Gangadharan, S. P., 2017, "Current Concepts in Severe Adult Tracheobronchomalacia: Evaluation and Treatment," J. Thorac. Dis., **9**(1), pp. E57–E66.
[2] Carden, K. A., Boiselle, P. M., Waltz, D. A., and Ernst, A., 2005, "Tracheomalacia and Tracheobronchomalacia in Children and Adults: An In-Depth Review," Chest, **127**(3), pp. 984–1005.
[3] Leong, P., Tran, A., Rangaswamy, J., Ruane, L. E., Fernando, M. W., MacDonald, M. I., Lau, K. K., and Bardin, P. G., 2017, "Expiratory Central Airway Collapse in Stable COPD and During Exacerbations," Respir. Res., **18**(1), p. 163.
[4] Chetambath, R., 2016, "Tracheobronchomalacia in Obstructive Airway Diseases," Lung India, **33**(4), pp. 451–452.
[5] Newell, J. D. J., Fuld, M. K., Allmendinger, T., Sieren, J. P., Chan, K.-S., Guo, J., and Hoffman, E. A., 2015, "Very Low-Dose (0.15 mGy) Chest CT Protocols Using the COPDGENE 2 Test Object and a Third-Generation Dual-Source CT

Scanner With Corresponding Third-Generation Iterative Reconstruction Software," Invest. Radiol., **50**(1), pp. 40–45.
[6] Weinstein, D. J., Hull, J. E., Ritchie, B. L., Hayes, J. A., and Morris, M. J., 2016, "Exercise-Associated Excessive Dynamic Airway Collapse in Military Personnel," Ann. Am. Thorac. Soc., **13**(9), pp. 1476–1482.
[7] Loring, S. H., O'Donnell, C. R., Feller-Kopman, D. J., and Ernst, A., 2007, "Central Airway Mechanics and Flow Limitation in Acquired Tracheobronchomalacia," Chest, **131**(4), pp. 1118–1124.
[8] Ellingsen, I., and Holmedahl, N. H., 2014, "Does Excessive Dynamic Airway Collapse Have Any Impact on Dynamic Pulmonary Function Tests?," J. Bronchology Interventional Pulmonol., **21**(1), pp. 40–46.
[9] Wall, W. A., and Rabczuk, T., 2008, "Fluid–Structure Interaction in Lower Airways of CT-Based Lung Geometries," Int. J. Numer. Methods Fluids, **57**(5), pp. 653–675.
[10] Xia, G., Tawhai, M. H., Hoffman, E. A., and Lin, C. L., 2010, "Airway Wall Stiffening Increases Peak Wall Shear Stress: A Fluid-Structure Interaction Study in Rigid and Compliant Airways," Ann. Biomed. Eng., **38**(5), pp. 1836–1853.
[11] Malvè, M., del Palomar, A. P., López-Villalobos, J. L., Ginel, A., and Doblaré, M., 2010, "FSI Analysis of the Coughing Mechanism in a Human Trachea," Ann. Biomed. Eng., **38**(4), pp. 1556–1565.
[12] Hollister, S. J., Hollister, M. P., and Hollister, S. K., 2017, "Computational Modeling of Airway Instability and Collapse in Tracheomalacia," Respir. Res., **18**(1), p. 62.
[13] Eskandari, M., Arvayo, A. L., and Levenston, M. E., 2018, "Mechanical Properties of the Airway Tree: Heterogeneous and Anisotropic Pseudoelastic and Viscoelastic Tissue Responses," J. Appl. Physiol., **125**(3), pp. 878–888.
[14] Miyawaki, S., Hoffman, E. A., and Lin, C. L., 2016, "Effect of Static vs. dynamic Imaging on Particle Transport in CT-Based Numerical Models of Human Central Airways," J. Aerosol Sci., **100**, pp. 129–139.
[15] Yin, Y., Choi, J., Hoffman, E. A., Tawhai, M. H., and Lin, C.-L., 2013, "A Multiscale MDCT Image-Based Breathing Lung Model With Time-Varying Regional Ventilation," J. Comput. Phys., **244**, pp. 168–192.
[16] Choi, S., Miyawaki, S., and Lin, C. L., 2018, "A Feasible Computational Fluid Dynamics Study for Relationships of Structural and Functional Alterations With Particle Depositions in Severe Asthmatic Lungs," Comput. Math. Methods Med., **2018**, p. 6564854.
[17] Ibrahim, G., Hainsworth, S. V., and Rona, A., 2012, "Airflow Simulation Through a Dynamic Subject-Specific Model of the Central Airways," International Conference on Applications of Fluid Engineering, Greater Noida, India, Sept. 20–22, pp. 1–6.
[18] Yin, Y., Hoffman, E. A., Ding, K., Reinhardt, J. M., and Lin, C. L., 2011, "A Cubic b-Spline-Based Hybrid Registration of Lung CT Images for a Dynamic Airway Geometric Model With Large Deformation," Phys. Med. Biol., **56**(1), pp. 203–218.
[19] Yin, Y., Choi, J., Hoffman, E. A., Tawhai, M. H., and Lin, C. L., 2010, "Simulation of Pulmonary Air Flow With a Subject-Specific Boundary Condition," J. Biomech., **43**(11), pp. 2159–2163.
[20] Murgu, S., and Stoy, S., 2016, "Excessive Dynamic Airway Collapse: A Standalone Cause of Exertional Dyspnea?," Ann. Am. Thorac. Soc., **13**(9), pp. 1437–1439.
[21] Dowdy, S. M., Wearden, S., and Chilko, D. M., 2004, *Statistics for Research*, Wiley, Hoboken, NJ.
[22] Kundu, P. K., Cohen, I. M., and Dowling, D. W., 2012, *Fluid Mechanics*, Academic Press, Waltham, MA.
[23] Sul, B., Oppito, Z., Jayasekera, S., Vanger, B., Zeller, A., Morris, M., Ruppert, K., Altes, T., Rakesh, V., Day, S., Robinson, R., Reifman, J., and Wallqvist, A., 2018, "Assessing Airflow Sensitivity to Healthy and Diseased Lung Conditions in a Computational Fluid Dynamics Model Validated In Vitro," ASME J. Biomech. Eng., **140**(5), p. 051009.
[24] Loudon, C., and Tordesillas, A., 1998, "The Use of the Dimensionless Womersley Number to Characterize the Unsteady Nature of Internal Flow," J. Theor. Biol., **191**(1), pp. 63–78.
[25] Sul, B., Wallqvist, A., Morris, M. J., Reifman, J., and Rakesh, V., 2014, "A Computational Study of the Respiratory Airflow Characteristics in Normal and Obstructed Human Airways," Comput. Biol. Med., **52**, pp. 130–143.
[26] Sidhaye, V. K., Schweitzer, K. S., Caterina, M. J., Shimoda, L., and King, L. S., 2008, "Shear Stress Regulates Aquaporin-5 and Airway Epithelial Barrier Function," Proc. Natl. Acad. Sci. U. S. A., **105**(9), pp. 3345–3350.
[27] Comerford, A., Förster, C., and Wall, W. A., 2010, "Structured Tree Impedance Outflow Boundary Conditions for 3D Lung Simulations," ASME J. Biomech. Eng., **132**(8), p. 081002.
[28] Kuprat, A. P., Kabilan, S., Carson, J. P., Corley, R. A., and Einstein, D. R., 2013, "A Bidirectional Coupling Procedure Applied to Multiscale Respiratory Modeling," J. Comput. Phys., **244**, pp. 148–167.
[29] Wall, W. A., Wiechert, L., Comerford, A., and Rausch, S., 2010, "Towards a Comprehensive Computational Model for the Respiratory System," Int. J. Numer. Meth. Biomed. Eng., **26**(7), pp. 807–827.
[30] Boiselle, P. M., Michaud, G., Roberts, D. H., Loring, S. H., Womble, H. M., Millett, M. E., and O'Donnell, C. R., 2012, "Dynamic Expiratory Tracheal Collapse in COPD: Correlation With Clinical and Physiologic Parameters," Chest, **142**(6), pp. 1539–1544.
[31] Rutten, M., Ciet, P., van den Biggelaar, R., Oussoren, E., Langendonk, J. G., van der Ploeg, A. T., and Langeveld, M., 2016, "Severe Tracheal and Bronchial Collapse in Adults With Type II Mucopolysaccharidosis," Orphanet J. Rare Dis., **11**, p. 50.
[32] Kolanjiyil, A. V., Kleinstreuer, C., and Sadikot, R. T., 2017, "Computationally Efficient Analysis of Particle Transport and Deposition in a Human Whole-Lung-Airway Model—Part II: Dry Powder Inhaler Application," Comput. Biol. Med., **84**, pp. 247–253.
[33] Kolanjiyil, A. V., and Kleinstreuer, C., 2017, "Computational Analysis of Aerosol-Dynamics in a Human Whole-Lung Airway Model," J. Aerosol Sci., **114**, pp. 301–316.
[34] Kannan, R., Guo, P., and Przekwas, A., 2016, "Particle Transport in the Human Respiratory Tract: Formulation of a Nodal Inverse Distance Weighted Eulerian–Lagrangian Transport and Implementation of the Wind–Kessel Algorithm for an Oral Delivery," Int. J. Numer. Meth. Biomed. Eng., **32**(6), p. e02746.
[35] Suh, Y., and Park, J. Y., 2018, "Effect of Off-Plane Bifurcation Angles of Primary Bronchi on Expiratory Flows in the Human Trachea," Comput. Biol. Med., **95**, pp. 63–74.
[36] De Lange, E. E., Altes, T. A., Patrie, J. T., Parmar, J., Brookeman, J. R., Mugler, J. P., III, and Platts-Mills, T. A., 2007, "The Variability of Regional Airflow Obstruction Within the Lungs of Patients With Asthma: Assessment With Hyperpolarized Helium-3 Magnetic Resonance Imaging," J. Allergy Clin. Immunol., **119**(5), pp. 1072–1078.
[37] Newell, J., Hoffman, E., Albert, M., and Couch, M., 2017, "CT and MRI Gas Ventilation Imaging of the Lungs," *Hyperpolarized and Inert Gas MRI*, Elsevier, Cambridge, MA, pp. 211–222.
[38] Thomen, R. P., Sheshadri, A., Quirk, J. D., Kozlowski, J., Ellison, H. D., Szczesniak, R. D., Castro, M., and Woods, J. C., 2015, "Regional Ventilation Changes in Severe Asthma After Bronchial Thermoplasty With 3He MR Imaging and CT," Radiology, **274**(1), pp. 250–259.
[39] Murgu, S. D., and Colt, H. G., 2006, "Tracheobronchomalacia and Excessive Dynamic Airway Collapse," Respirology, **11**(4), pp. 388–406.
[40] Zafar, M. A., Mulhall, A. M., Eschenbacher, W., Kaul, A., Benzaquen, S., and Panos, R. J., 2017, "Manometry Optimized Positive Expiratory Pressure (MOPEP) in Excessive Dynamic Airway Collapse (EDAC)," Respir. Med., **131**, pp. 179–183.
[41] Karmakar, A., Pate, M. B., Solowski, N. L., Postma, G. N., and Weinberger, P. M., 2015, "Tracheal Size Variability Is Associated With Sex: Implications for Endotracheal Tube Selection," Ann. Otol. Rhinol. Laryngol., **124**(2), pp. 132–136.